Enhancement of radiation hardness of InP-based HEMT with double Si-doped plane*

Ying-Hui Zhong(钟英辉)[1], Bo Yang(杨博)[1], Ming-Ming Chang(常明铭)[1], Peng Ding(丁芃)[2], Liu-Hong Ma(马刘红)[1], Meng-Ke Li(李梦珂)[1], Zhi-Yong Duan(段智勇)[1], Jie Yang(杨洁)[1,†], Zhi Jin(金智)[2,3], and Zhi-Chao Wei(魏志超)[3]

[1] *School of Physics and Microelectronics, Zhengzhou University, Zhengzhou* 450001, *China*
[2] *Institute of Microelectronics, Chinese Academy of Sciences, Beijing* 100029, *China*
[3] *China Academy of Space Technology, Beijing* 100086, *China*

(Received 22 October 2019; revised manuscript received 25 December 2019; accepted manuscript online 9 January 2020)

An anti-radiation structure of InP-based high electron mobility transistor (HEMT) has been proposed and optimized with double Si-doped planes. The additional Si-doped plane under channel layer has made a huge promotion in channel current, transconductance, current gain cut-off frequency, and maximum oscillation frequency of InP-based HEMTs. Moreover, direct current (DC) and radio frequency (RF) characteristic properties and their reduction rates have been compared in detail between single Si-doped and double Si-doped structures after 75-keV proton irradiation with dose of 5×10^{11} cm^{-2}, 1×10^{12} cm^{-2}, and 5×10^{12} cm^{-2}. DC and RF characteristics for both structures are observed to decrease gradually as irradiation dose rises, which particularly show a drastic drop at dose of 5×10^{12} cm^{-2}. Besides, characteristic degradation degree of the double Si-doped structure is significantly lower than that of the single Si-doped structure, especially at large proton irradiation dose. The enhancement of proton radiation tolerance by the insertion of another Si-doped plane could be accounted for the tremendously increased native carriers, which are bound to weaken substantially the carrier removal effect by irradiation-induced defects.

Keywords: InP-based HEMT, anti-radiation, proton irradiation, Si-doped plane

PACS: 85.30.De, 73.61.Ey, 14.20.Dh **DOI:** 10.1088/1674-1056/ab6962

1. Introduction

In nearly several decades, many effective measures have been taken to extend Moore's law, such as advanced micro/nano-fabrication technologies, novel materials and structures.[1–3] Because of high carrier sheet density, high carrier peak drift velocity, and low-field mobility in InGaAs channel, InAlAs/InGaAs InP-based high electron mobility transistors (HEMTs) have stood out and become competitive alternatives with high frequency, low noise figure, superior gain performance, and so on.[4–6] Furthermore, benefiting from electron beam lithography (EBL) and molecular beam epitaxy (MBE) techniques, the current gain cut-off frequency ($f_{\rm T}$) and maximum oscillation frequency ($f_{\rm max}$) of InP-based HEMTs have been reported to be over than 700 GHz[7] and 1 THz,[8] respectively. Consequently, InP-based HEMTs become as potential candidates for various high speed circuits of transceiver systems in space applications, such as national defense, aerospace, and satellite radar.[9]

In harsh space environment, various high-energy particles and rays will inevitably lead to performance deterioration of devices and even abnormality of electronic systems.[10,11] Especially, proton is one of the main particles in space irradiation environment. Considering mature high technology, low manufacturing cost, and broad usage, researches about proton irradiation effect and hardness techniques are mainly concentrated on Si-based complementary metal–oxide–semiconductor transistor (CMOS) and silicon on insulator (SOI) devices.[12,13] Nevertheless, there are some existing exploratory research on the proton irradiation effects of the various III–V materials devices.[14–17] As a result, the degradation degree of the device characteristics after proton irradiation is directly related to the amount of vacancy defects which are caused by displacement effect, and this damage mechanism has gained wide consensus.[18]

The reliability research of III–V devices about proton irradiation rarely involves anti-radiation device structure and technology techniques. Admittedly, some anti-radiation measures have been proposed yet for III–V devices based on the above proton irradiation damage mechanism and heterojunction structure, that are the reduction of the body-traps in materials or substitution for current materials with high displacement threshold energy.[19] However, these irradiation hardness techniques will involve enormous constraint from either epitaxy technology or lattice mismatch.

In this paper, InP-based HEMT structure with double Si-doping planes has been put forward and optimized to increase the native carrier concentration and thus improve the proton irradiation tolerance. The DC and RF characteristics of In-

*Project supported by the National Natural Science Foundation of China (Grant Nos. 11775191, 61404115, 61434006, and 11475256) and the Promotion Funding for Excellent Young Backbone Teacher of Henan Province, China (Grant No. 2019GGJS017).

†Corresponding author. E-mail: yangjie_zzu2@163.com

AlAs/InGaAs InP-based HEMTs with single and double Si-doped plane have been investigated comprehensively by two-dimensional digital simulation. Additionally, their properties of radiation hardness have been studied in detail before and after 75-keV proton irradiation with dose of 5×10^{11} cm^{-2}, 1×10^{12} cm^{-2}, and 5×10^{12} cm^{-2}.

2. Device structure and physical model

Figure 1 shows the schematic cross-section of InP-based HEMTs. The epitaxial structure with single Si-doping plane is almost consistent with previous device fabrication,[20,21] as shown in Fig. 1(a). The epitaxial layers from bottom to top consist of a 500-nm semi-insulating InP substrate, a 500-nm InAlAs buffer, a 15-nm InGaAs channel, a 3-nm unstrained InAlAs spacer layer, a Si-doped plane which provides two-dimensional electron gas (2DEG), and the doping concentration is 5×10^{12} cm^{-2}, a 12-nm-thick unstrained lnAlAs Schottky barrier layer, and a 30-nm highly Si-doped cap layer with the doping concentration of 3×10^{19} cm^{-3}. And the gate length is 100 nm, the gate–drain distance is 1 μm. All InAlAs layers are lattice matched with the InP substrate. On the basis, device structure with double Si-doping planes is designed and optimized to maximum the proton radiation tolerance in DC and RF characteristics, as illustrated in Fig. 1(b). Particularly, an additional Si-doped plane is inserted under channel layer with 3-nm-thick unstrained InAlAs spacer layer.

Reasonable physical models are used to describe the device performances, including hydrodynamic transport model, Shockley–Read–Hall recombination, Auger recombination, radiative recombination, density gradient model, and high field-dependent mobility. And, the hydrodynamic transport model precisely describes many non-equilibrium conditions such as quasi-ballistic transport in thin regions and velocity overshoot effect in depleted regions. Shockley–Read–Hall recombination, Auger recombination, and radiative recombination models are adopted to describe carrier exchange process with the impurity defects in the band-gap. The density gradient model of eQuantumPotential is introduced to depict the quantum effect of 2DEG in InGaAs channel region. The doping and high field-dependent mobility model is used to describe the degradation of electron mobility. Moreover, the irradiation-induced vacancies by displacement effect after proton irradiation are considered self-consistently through solving Poisson and current continuity equations as follows:[22,23]

$$\nabla^2\varphi = -\frac{q}{\varepsilon}\left[p - n + N_{\rm D}^{+} - N_{\rm A}^{-}\right] - \frac{\rho_{\rm trap}}{\varepsilon}, \tag{1}$$

$$\begin{aligned}
\frac{\partial_{\rm n}}{\partial_{\rm t}} &= \frac{1}{q}\nabla\cdot J_{\rm n},\\
\frac{\partial_{\rm p}}{\partial_{\rm t}} &= \frac{1}{q}\nabla\cdot J_{\rm p},\\
J_{\rm n} &= -q\mu_{\rm n} n\nabla\Phi_{\rm n},
\end{aligned} \tag{2}$$

$$J_{\rm p} = q\mu_{\rm p} p\nabla\Phi_{\rm p}, \tag{3}$$

where $N_{\rm D}^{+}$ and $N_{\rm A}^{-}$ are the ionized donor and acceptor concentration, which include background doping and also the ionized traps caused by proton irradiation. $\rho_{\rm trap}$ is the charge density induced by vacancies. $J_{\rm n}$ and $J_{\rm p}$ are electron and hole current densities. $\mu_{\rm n}$ and $\mu_{\rm p}$ are the electron and hole mobilities. $\Phi_{\rm n}$ and $\Phi_{\rm p}$ are the electron and hole quasi-Fermi levels.

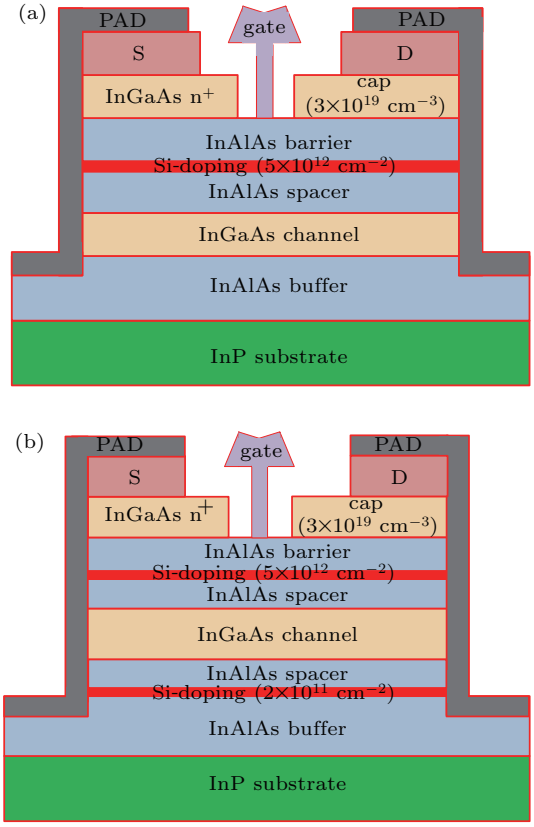

Fig. 1. Schematic cross-section of InP-based HEMTs: (a) single Si-doping plane; (b) double Si-doping plane.

3. Simulation results and discussion

With the increasing of proton energy, the ultimate stopping position of incident protons in target object will undoubtedly transform from gate metal to hetero-junction layer, and eventually protons will pass through the entire material layers. Consequently, the number of induced defects in hetero-junction region increases firstly and reaches the largest value at about 75 keV.[24] To make a comprehensive impact of proton irradiation on device, the incident proton energy was set as 75 keV with dose of 5×10^{11} cm^{-2}, 1×10^{12} cm^{-2}, and 5×10^{12} cm^{-2}.

The output drain current ($I_{\rm DS}$) *versus* drain–source voltage ($V_{\rm DS}$) characteristics of two structures are assessed before and after 75-keV proton irradiation, as shown in Fig. 2. $V_{\rm DS}$ sweeps positively from 0 V to 1.5 V in steps of 0.075 V, while gate–source voltage ($V_{\rm GS}$) is assigned as a constant of 0 V. From the output characteristics curves, additional Si-doped

plane makes approximately a 30% increase to channel current. Channel current for both two structures were observed to decrease gradually as irradiation dose rises, which especially show a drastic drop at dose of 5×10^{12} cm^{-2}. Furthermore, the reduction rates of saturation output drain current ($\Delta I_{\mathrm{D,sat}}$) were exactly computed and shown in Fig. 3. With the irradiation dose increasing from 5×10^{11} cm^{-2} to 5×10^{12} cm^{-2}, $I_{\mathrm{D,sat}}$ of single Si-doped structure has deteriorated by 4.5%–45.2%, which has dramatically fallen down to 2.97%–32.1% for double Si-doped structure. Obviously, the additional Si-doped plane has effectively improved the degradation degree of channel current, and the dominance becomes more and more significant at large proton irradiation dose.

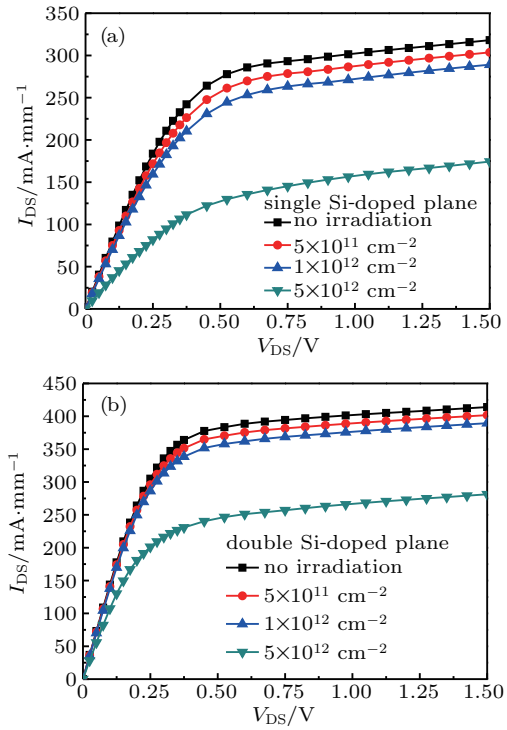

Fig. 2. Output characteristic of InP-based HEMTs before and after proton irradiations with dose of 5×10^{11} cm^{-2}, 1×10^{12} cm^{-2}, and 5×10^{12} cm^{-2}. (a) Single Si-doped structure; (b) double Si-doped structure.

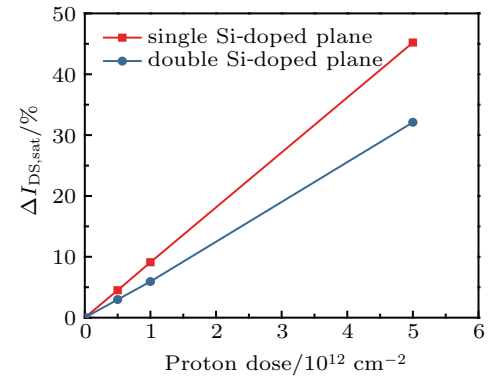

Fig. 3. Reduction rates of saturation output drain current for devices with single Si-doped plane and double Si-doped plane.

Figure 4 demonstrates the extrinsic transconductance (g_{m}) and channel current of InP-based HEMTs at V_{DS} of 1.5 V. The maximum transconductance ($g_{\mathrm{m,max}}$) improves from 667.081 mS/mm to 674.829 mS/mm by introducing another Si-doped plane, increasing by 1.2%. The relatively smaller increment than output drain current may be accounted to the lager distance from gate terminal to the Si-doped plane under channel layer. With irradiation dose rising up from 5×10^{11} cm^{-2} to 5×10^{12} cm^{-2}, the reduction rate of maximum transconductance ($\Delta g_{\mathrm{m,max}}$) increases from 2.1% to 23.8% for double Si-doped structure, likewise, the value of single Si-doped structure changes positively from 2.9% to 32.3%. These also indicate that the degradation degree of InP-based HEMTs with double Si-doped plane is better than that of single Si-doped structure before and after proton irradiation, especially at large proton irradiation dose.

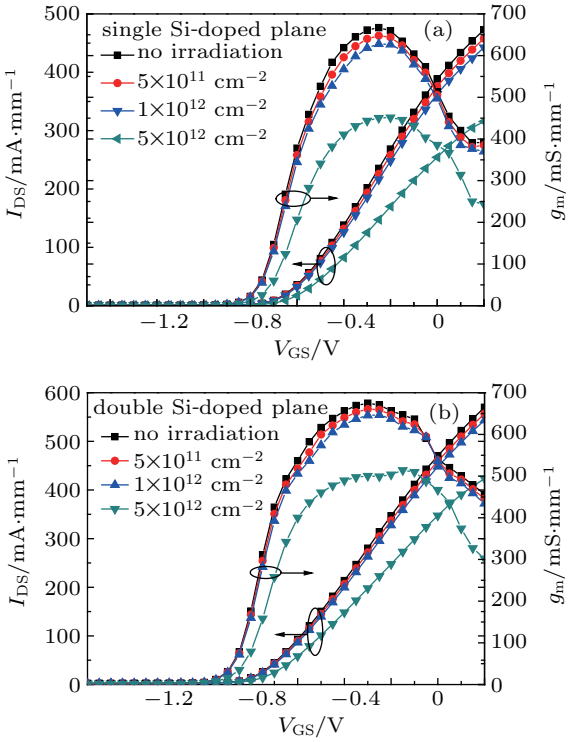

Fig. 4. Transfer characteristics of InP-based HEMTs before and after proton irradiations with dose of 5×10^{11} cm^{-2}, 1×10^{12} cm^{-2}, and 5×10^{12} cm^{-2}. (a) Single Si-doped structure; (b) double Si-doped structure.

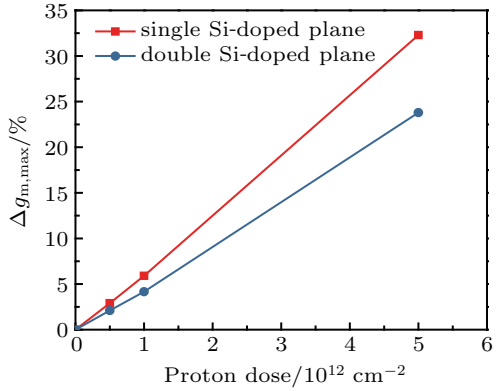

Fig. 5. Reduction rates of maximum transconductance for devices with single Si-doped plane and double Si-doped planes.

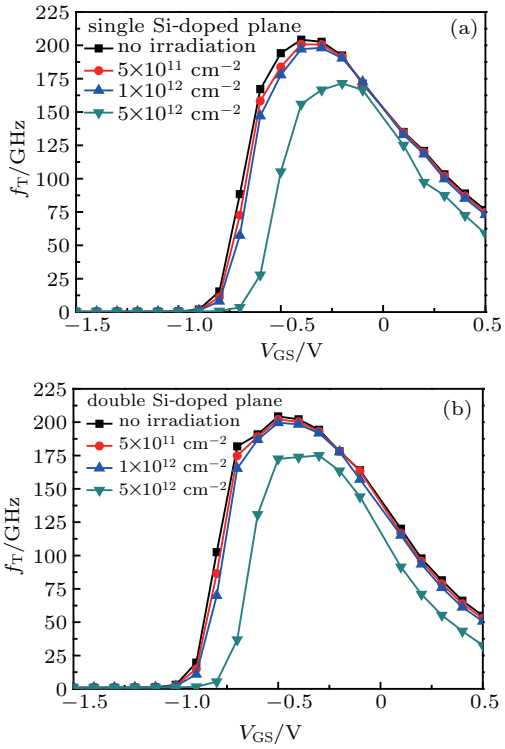

Fig. 6. f_T of InP-based HEMTs before and after proton irradiations with dose of 5×10^{11} cm^{-2}, 1×10^{12} cm^{-2}, and 5×10^{12} cm^{-2}. (a) Single Si-doped structure; (b) double Si-doped structure.

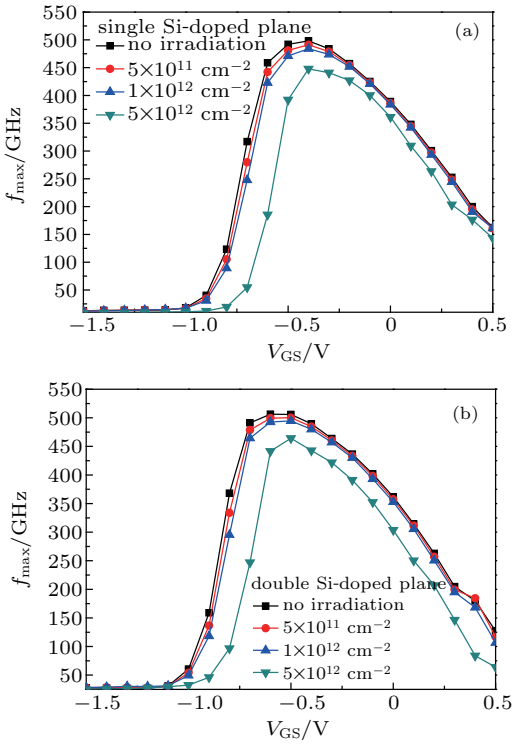

Fig. 7. f_{max} of InP-based HEMTs before and after proton irradiations with dose of 5×10^{11} cm^{-2}, 1×10^{12} cm^{-2}, and 5×10^{12} cm^{-2}. (a) Single Si-doped structure; (b) double Si-doped structure.

The f_T and f_{max} are vital parameters for high speed device application. Exactly, f_{max} affects the device power gain of analog circuit, while f_T determines the switching speed of digital circuit. Figures 6 and 7 have exhibited that f_T and f_{max} *versus* V_{GS} for InP-based HEMTs before and after 75-keV proton irradiations. As illustrated in Fig. 8, the frequency characteristics of double Si-doped structure have just shown a slight improvement, which is mainly due to the increase of capacitance in double Si-doped structure. The frequency properties for both two structures are detected to decrease gradually

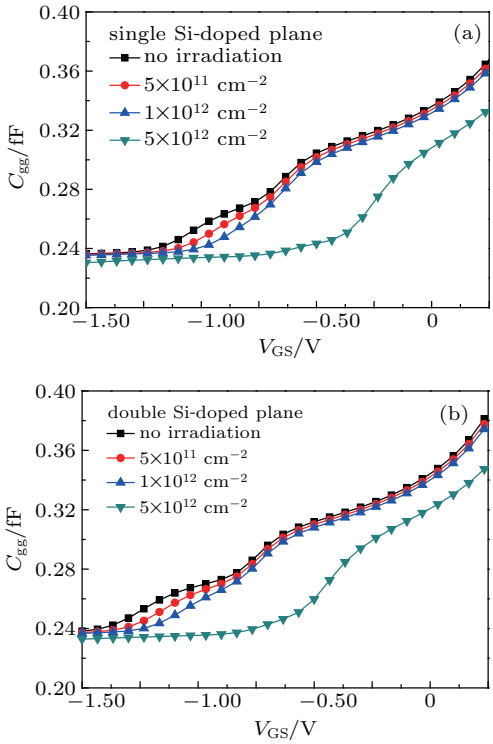

Fig. 8. C_{gg} of InP-based HEMTs before and after proton irradiations with dose of 5×10^{11} cm^{-2}, 1×10^{12} cm^{-2}, and 5×10^{12} cm^{-2}. (a) Single Si-doped structure; (b) double Si-doped structure.

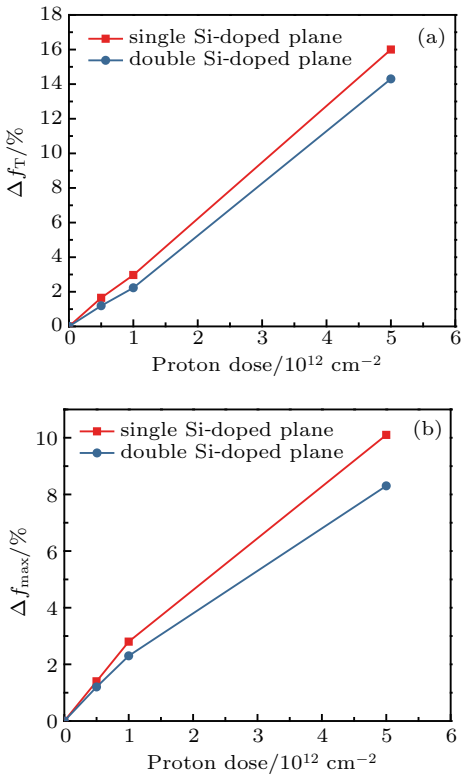

Fig. 9. Reduction rates of frequency characteristics for devices with single Si-doped plane and double Si-doped planes: (a) Δf_T; (b) Δf_{max}.

as irradiation dose rises, and a sharply decline has begun to emerge at dose of 5×10^{12} cm^{-2}. The reduction rates of f_T and f_{max} (Δf_T and Δf_{max}) have been comparatively obtained and shown in Fig. 9. Apparently, the degradation degree of RF characteristics of double Si-doped structure is clearly lower than that of single Si-doped structure at the same irradiation dose.

The electron concentration in the channel region and their reduction rates are investigated for two kinds of structures before and after 75-keV proton irradiation, as shown in Fig. 10. The electron concentration decreases with the increasing of irradiation dose for both two device structures. Moreover, the double Si-doped structure demonstrates superior proton radiation-tolerance in carrier concentration. As the proton irradiation dose surges higher, vacancy defects in larger number are necessarily induced in InAlAs/InGaAs hetero-junction region. These defects may act as carrier recombination centers or trapping centers, and cause a decrease in carrier sheet density by carrier removal effect. Consequently, DC and RF characteristics of devices may deteriorate more seriously with irradiation dose. An additional Si-doping plane inserted under channel layer with a thin spacer layer has tremendously increased the native carrier concentration in channel region, which is bound to weaken substantially the carrier removal effect by induced defects, and finally improved the proton radiation tolerance in DC and RF characteristics.

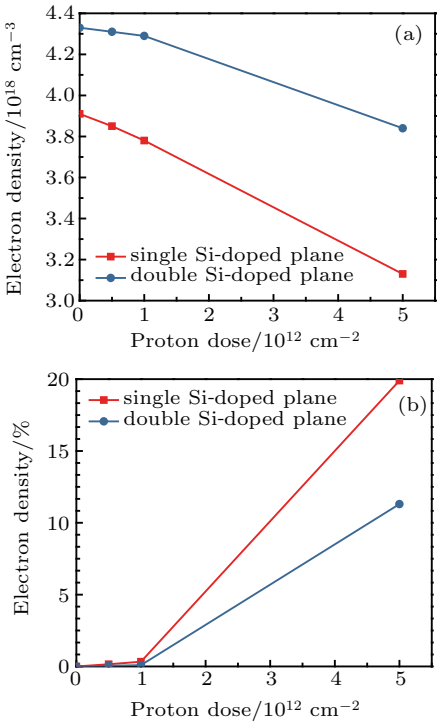

Fig. 10. 2DEG for InP-based HEMTs with single Si-doped plane and double Si-doped planes. (a) Elecron concentration; (b) reduction rates.

4. Conclusion and perspectives

In summary, the double Si-doped structure of InP-based HEMT was designed and optimized to improve the proton irradiation tolerance, which eventually has demonstrated superior DC and RF characteristics than traditional single Si-doped structure. Moreover, the inserted another Si-doped plane under channel layer increases the native carrier concentration in channel region, which weakens substantially the carrier removal effect by irradiation-induced defects. Consequently, proton radiation tolerance of double Si-doped structure has been greatly improved with lower reduction rates of DC and RF properties, especially at large irradiation dose. These studies could provide theoretical basis and technical support for irradiation harden design of InP-based HEMTs and integrated circuits, so as to further improve the stability and durability of relative electronic systems.

References

[1] Wang W, Su Y F, Liu C R, Li D X, Wang P and Duan Z Y 2015 *Chin. Phys. Lett.* **32** 128102
[2] Shangguan L, Ma L, Li M, Peng W, Zhong Y, Su Y and Duan Z 2018 *J. Phys. D: Appl. Phys.* **51** 185603
[3] Ma L H, Han W H, Zhao X S, Guo Y Y, Dou Y M and Yang F H 2018 *Chin. Phys. B* **27** 088106
[4] Jo H B, Baek J M, Yun D Y, Son S W, Lee J H, Kim T W, Kim D H, Tsutsumi T, Sugiyama H and Matsuzaki H 2018 *IEEE Electron Dev. Lett.* **39** 1640
[5] Baek J M, Son S W, Park J H, Park J K, Kwak J G, Yoon J, Bang D S, Lee J H, Kim T and Kim D H 2018 *Solid State Electron.* **147** 58
[6] Zhong Y H, Li K K, Li X J and Jin Z 2015 *J. Infrared Millim. Waves* **34** 0668
[7] Ajayan J, Ravichandran T, Prajoon P, Pravin J C and Nirmal D 2018 *J. Comput. Electron.* **17** 265
[8] Mei X, Yoshida W, Lange M, Lee J, Zhou J, Liu P H, Leong K, Zamora A, Padilla J, Sarkozy S, Lai R and Deal W R 2015 *IEEE Electron Dev. Lett.* **36** 327
[9] Takahashi T, Kawano Y, Makiyama K, Shiba S, Sato M, Nakasha Y and Hara N 2017 *IEEE T. Electron. Dev.* **64** 89
[10] Pearton S J, Deist R, Ren F, Liu L, Polyakov A Y and Kim J 2013 *J. Vac. Technol. A* **31** 050801
[11] Douglas E A, Bielejec E, Frenzer P, Yates B R, Pearton S J, Lo C F, Liu L, Kang T S and Ren F 2013 *J. Vac. Technol. B* **31** 021205
[12] Carniti P, Cassina L, Gotti C, Maino M and Pessina G 2016 *Nucl. Instrum. Methods Phys. Res. Sect. A* **824** 258
[13] Kurachi I, Kobayashi K, Okihara M, Kasai H, Hatsui T, Hara K, Miyoshi T and Arai Y 2015 *IEEE T. Electron. Dev.* **62** 2371
[14] Tunhuma S M, Auret F D, Legodi M J and Diale M 2016 *J. Appl. Phys.* **119** 145705
[15] Anderson T J, Koehler A D, Greenlee J D, Weaver B D, Mastro M A, Hite J K, Eddy C R, Kub F J and Hobart K D 2014 *IEEE Electron Dev. Lett.* **35** 826
[16] Hwang Y H, Li S, Hsieh Y L, Ren F, Pearton S J, Patrick E, Law M E and Smith D J 2014 *Appl. Phys. Lett.* **104** 082106
[17] Sun S, Chang M, Zhang C, Cheng C, Li Y, Zhong Y, Ding P, Jin Z and Wei Z 2018 *Phys. Status Solidi-R* **12** 1800027
[18] Sun S, Chang M, Li M, Ma L, Zhong Y, Li Y, Ding P, Jin Z and Wei Z 2019 *Chin. Phys. B* **28** 078501
[19] Weaver B D, Anderson T J, Koehler A D, Greenlee J D, Hite J K, Shahin D I, Kub F J and Hobart K D 2016 *ECS J. Solid State Sci. Technol.* **5** Q208
[20] Zhong Y, Wang W, Sun S, Ding P and Jin Z 2014 *Phys. Status Solidi A* **214** 1700411
[21] Zhong Y H, Yang J, Li X J, Ding P and Jin Z 2015 *J. Korean Phys. Soc.* **66** 1020
[22] Patrick E, Law M E, Liu L, Velez Cuervo C, Xi Y, Ren F and Pearton S J 2013 *IEEE T. Nucl. Sci.* **60** 4103
[23] Patrick E E, Choudhury M, Ren F, Pearton S J and Law M E 2015 *ECS J. Solid State Sci.* **4** Q21
[24] Sun S X, Wei Z C, Xia P H, Wang W B, Duan Z Y, Li Y X, Zhong Y H, Ding P and Jin Z 2018 *Chin. Phys. B* **27** 028502